Supporting Information

-for-

Exploring Ir-doped NiFe-LDH nanosheets via a pulsed laser for oxygen evolution kinetics: in situ Raman and DFT insights

Sieon Jung [a, ‡], Raja Arumugam Senthil [a, ‡], Ahreum Min [b, ‡], Anuj Kumar [c], Cheol Joo Moon [b], Gyeong Hwa Jeong [d], Tae Wu Kim [e,], Myong Yong Choi [a,b,]**

[a] *Department of Chemistry (BK21 FOUR), Research Institute of Natural Sciences, Gyeongsang National University, Jinju 52828, Republic of Korea*

[b] *Core-Facility Center for Photochemistry & Nanomaterials, Gyeongsang National University, Jinju 52828, Republic of Korea*

[c] *Nano-Technology Research Laboratory, Department of Chemistry, GLA University, Mathura, Uttar Pradesh 281406, India*

[d] *Research Institute for Green Energy Convergence Technology, Gyeongsang National University, Jinju, 52828, Republic of Korea*

[e] *Department of Chemistry, Mokpo National University, Muan-gun 58554, Republic of Korea*

* Corresponding author E-mail address: twkim@mnu.ac.kr (T. W. Kim) & mychoi@gnu.ac.kr (M. Y. Choi)

[‡] These authors contributed equally to this work

Characterization techniques

X-ray diffraction (XRD) measurements were performed on a Bruker D8 Advance A25 diffractometer (Germany) with Cu-Kα radiation (λ = 0.1541 nm) at a scan rate of 10°/min. Raman spectra were collected from a Horiba Jobin-Yvon Raman microscope (LabRAM, HR800). Scanning electron microscopy (SEM) and energy dispersive X-ray spectroscopy (EDS) images were measured on a TESCAN S-8000 scanning electron microscope (Czech Republic) coupled with an energy dispersive X-ray spectrometry (Ultim Max, Oxford). High-resolution transmission electron microscopy (HR-TEM) images were taken on a Talos F200X transmission electron microscope (FEI company, USA) under a working voltage of 200 kV. X-ray photoelectron spectroscopy (XPS) spectra were collected from an NEXSA G2 X-ray photoelectron spectrometer (Thermo Fisher Scientific, USA) with monochromatic Al-Kα radiation. Inductively coupled plasma pptical emission spectrometry (ICP) analysis was performed on an iCAP PRO XP Duo spectrometer (Thermo Fisher Scientific, USA). X-ray absorption near-edge structure (XANES) and Fourier transform (FT) extended X-ray absorption fine structure (EXAFS) data were collected at the Ir L_3-edge. This was achieved by employing a monochromatic X-ray absorption spectroscopic setup equipped with a Si (111) double-crystal monochromator and a silicon semiconductor detector. All data were acquired in the total-fluorescence-yield (TFY) mode under ambient atmospheric conditions. To determine the bond distance from the obtained EXAFS data, a systematic analysis was performed, involving the Fourier transform of k_3-weighed oscillation data within the EXAFS signal.

Electrochemical measurements

Tafel slope and EIS measurements

From the linear sweep voltammetry (LSV) plots, the Tafel plots were derived by plotting as overpotential versus log of current density. Subsequently, Tafel slopes can be determined by fitting the linear parts of Tafel plots using Tafel equation of $\eta = a + b\log(j)$, where, η, a, b and j indicates the overpotential, Tafel constant, Tafel slope and current density, correspondingly. Furthermore, the electrochemical impedance spectroscopy (EIS) tests were measured within the frequency range of 0.1-10^5 Hz at a fixed potential (V) vs. RHE.

Calculation of ECSA from the C_{dl} measurements

To calculate the electrochemical surface area (ECSA), the cyclic voltammetry (CV) curves were measured at different scan rates from 10 to 100 mv s^{-1} in the non-Faradic regions (0.95-1.05 V Vs. RHE). By plotting the $\Delta j/2$ at 1.0 V vs. RHE versus the scan rates, a linear trend was obtained and then, the slope is correspondent to the double layer capacitance (C_{dl}), as represented by an equation of $C_{dl} = d(\Delta j)/2d\nu$, where ν is the scan rate. After that, the electrochemical active surface area (ECSA) can be obtained from the equation of ECSA = C_{dl}/C_s*S, here, C_s is the specific capacitance of CC substrate (88 mF cm^{-2}) and S is the area of the working electrode (cm^2).

Calculation of turnover frequency (TOF)

Turnover frequency (TOF) values were calculated from the equation of TOF (s^{-1}) = $j\times N_A/(n\times S_A\times F)$, where, j is the current density at a given potential, N_A is the Avogadro's number (6.022×10^{23}), n is the number of electrons involved to produce one molecule of the product (in case of OER; 4 electrons are involved to generate O_2 molecule), F is the Faraday constant (96485 C mol^{-1}), and S_A is the amount of available active sites. The S_A is measured from the reduction part of CV curve under the equation of S_A = (Integrated area of reduction

part of the CV curve/scan rate)/charge of electron. The charge of electron is 1.602×10^{-19} C.

Calculation of mass activity

The mass activity of the catalysts is defined as the current density (in units of mA cm^{-2}) normalized by the mass of the active material in the catalyst (in units of mg). This can be expressed mathematically as: Mass activity = j/m, where, "j" represents the current density, and "m" represents the loading mass of the catalyst.

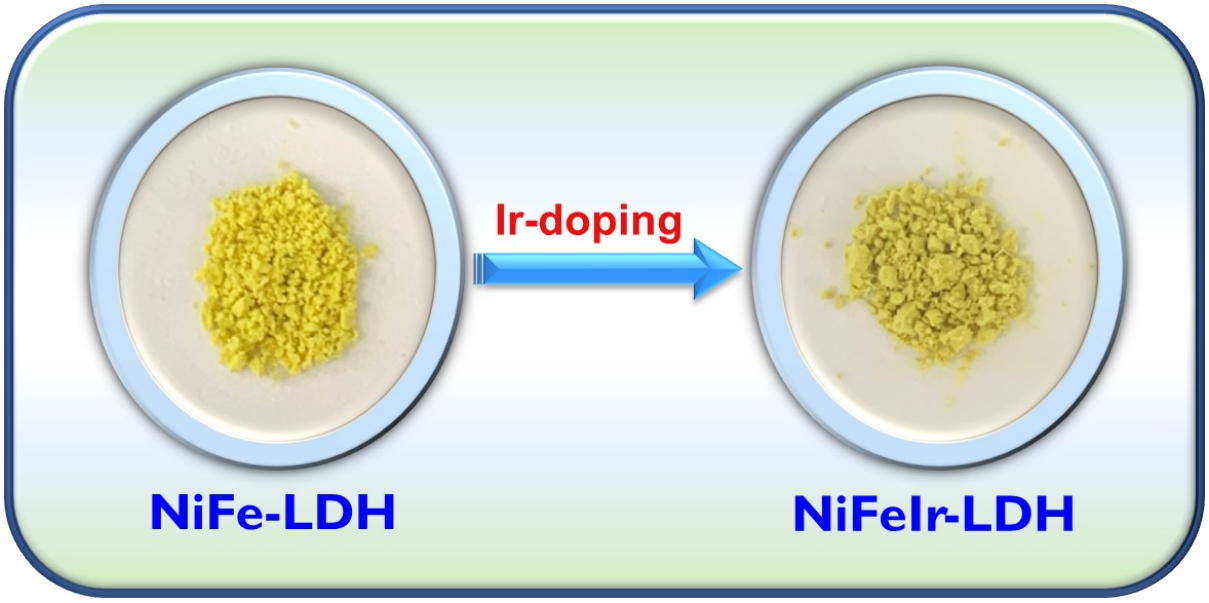

Fig. S1. The photographs of the as-synthesized NiFe-LDH and NiFeIr-LDH samples via PLI method.

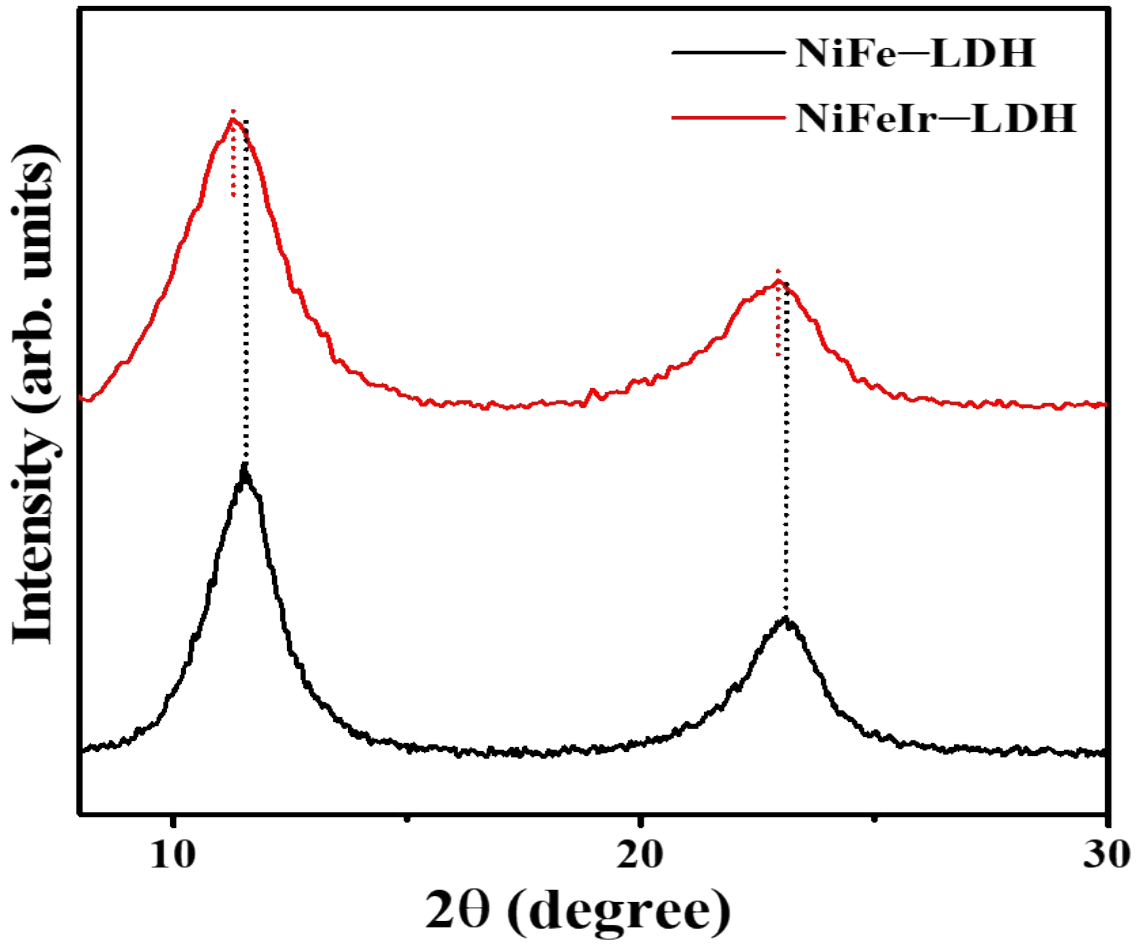

Fig. S2. The zoomed-in view of XRD patterns of the as-synthesized NiFe-LDH and NiFeIr-LDH nanosheets via PLI method.

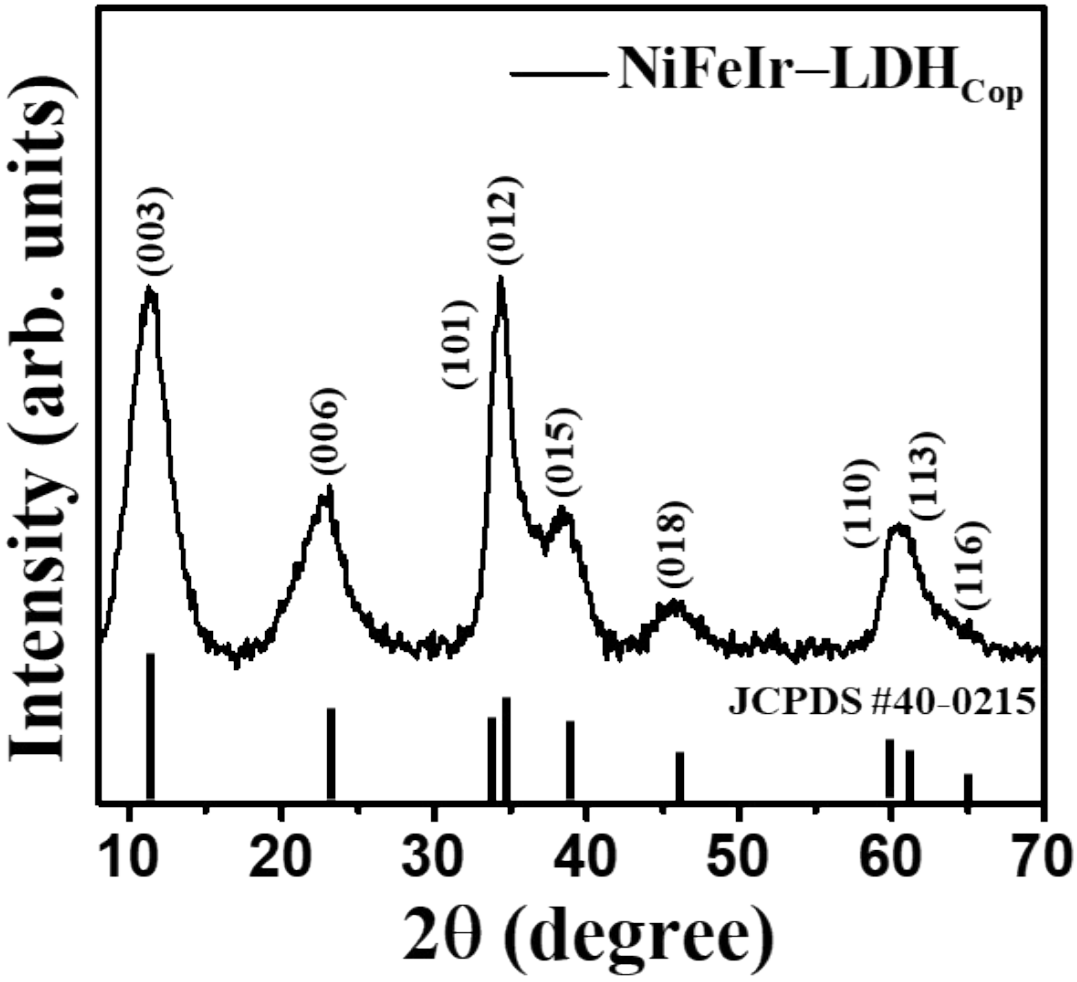

Figure S3. XRD pattern of the synthesized NiFeIr-LDH$_{Cop}$ nanosheets via co-precipitation method.

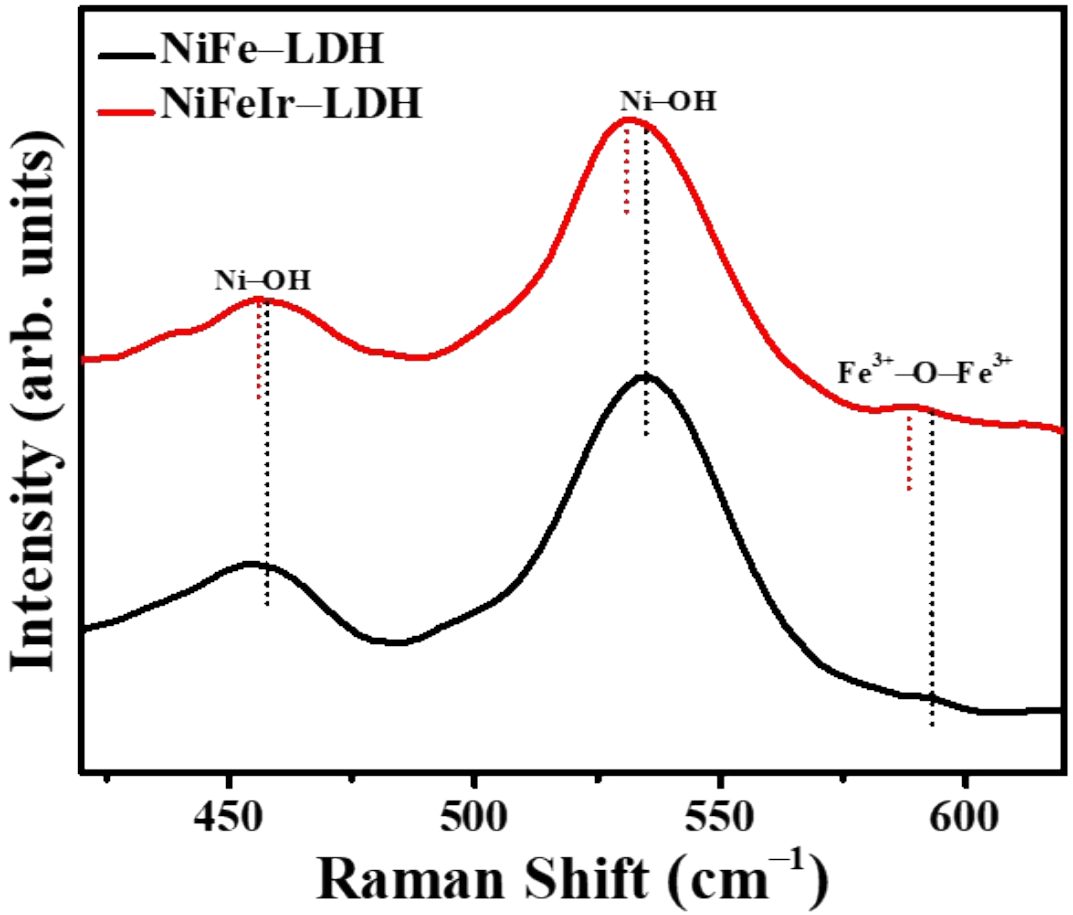

Fig. S4. The zoomed-in view of Raman spectra of the as-synthesized NiFe-LDH and NiFeIr-LDH nanosheets via PLI method.

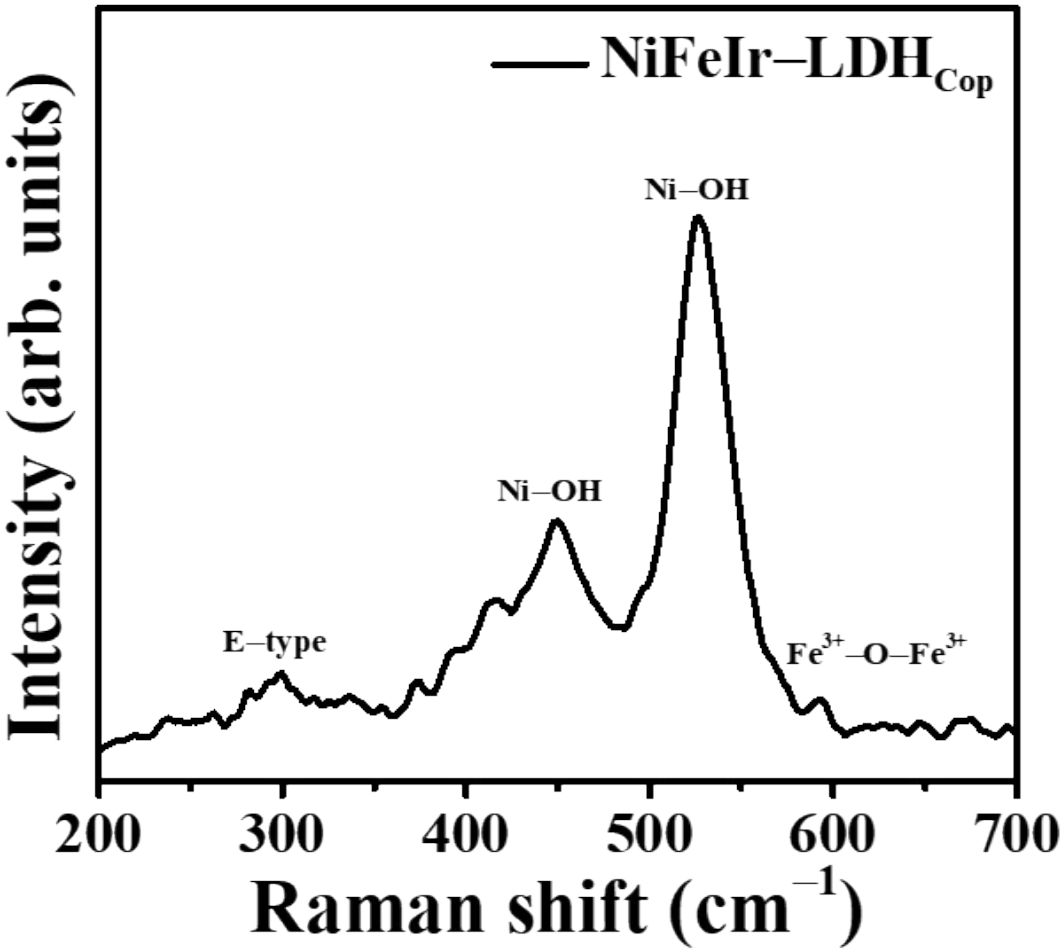

Fig. S5. Raman spectrum of the synthesized NiFeIr-LDH$_{Cop}$ nanosheets via co-precipitation method.

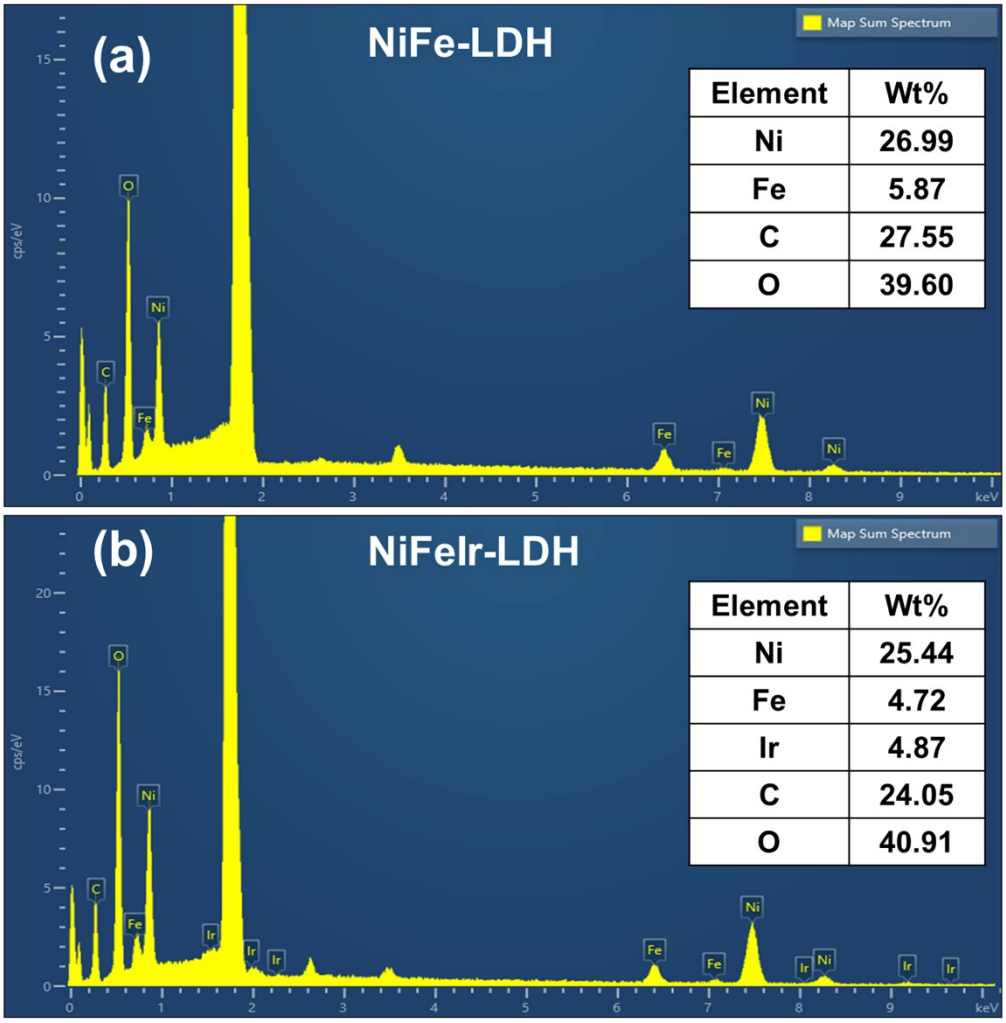

Fig. S6. EDS spectra of the as-synthesized (a) NiFe-LDH and (b) NiFeIr-LDH nanosheets via PLI method.

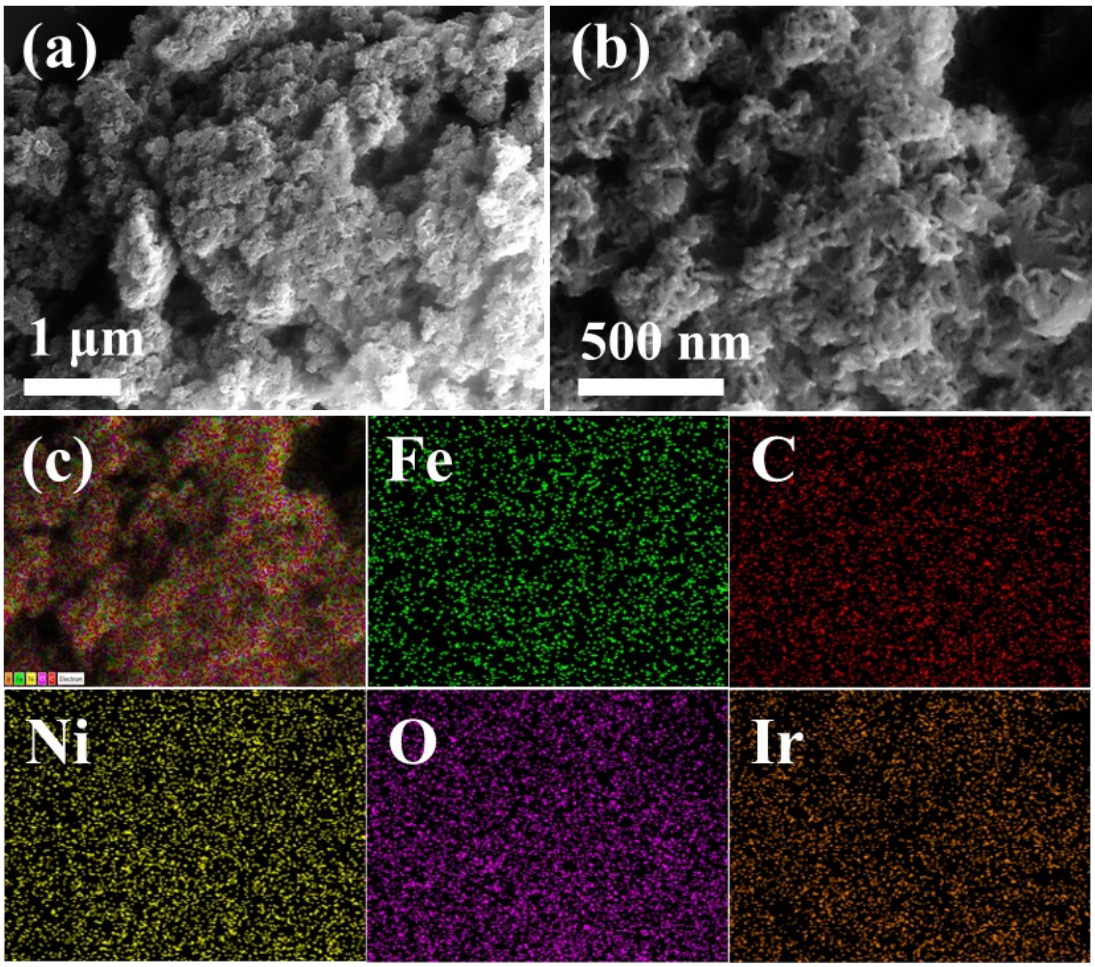

Fig. S7. (a,b) SEM and (c) EDS mapping images of the synthesized NiFeIr-LDH_{Cop} nanosheets via co-precipitation method.

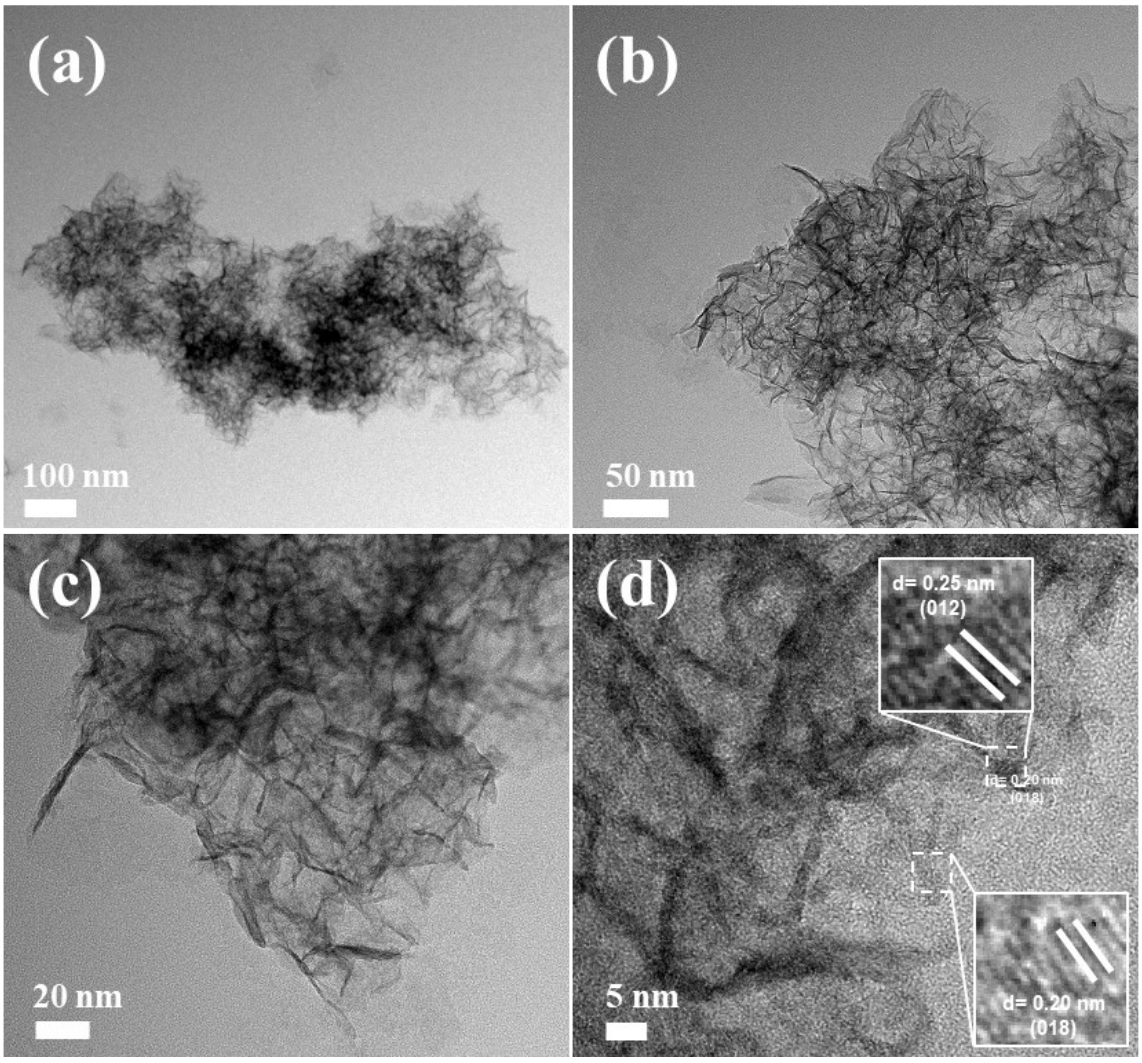

Fig. S8. HR-TEM images of the synthesized NiFeIr-LDH_{Cop} nanosheets via co-precipitation method.

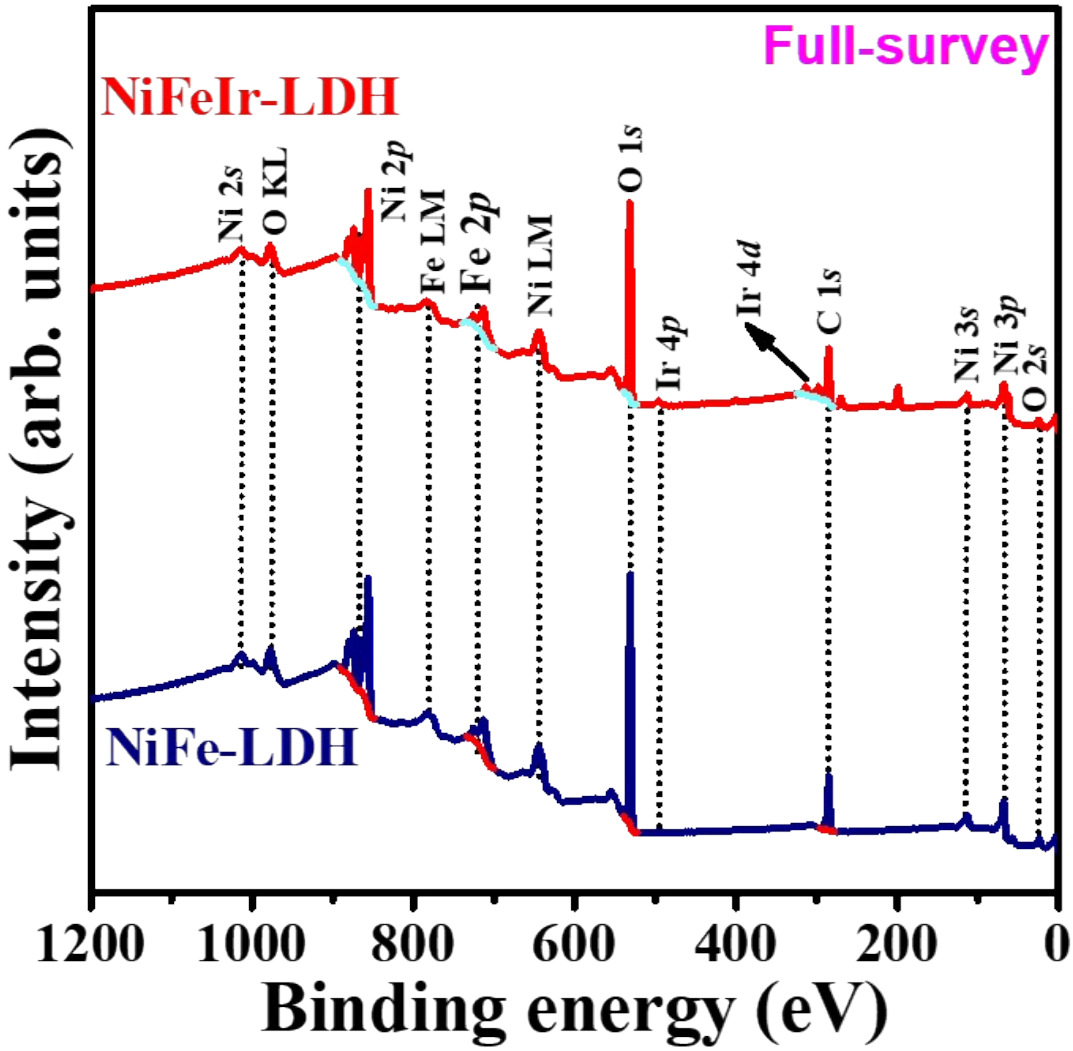

Fig. S9. XPS survey spectra of the synthesized NiFe-LDH and NiFeIr-LDH nanosheets via PLI method.

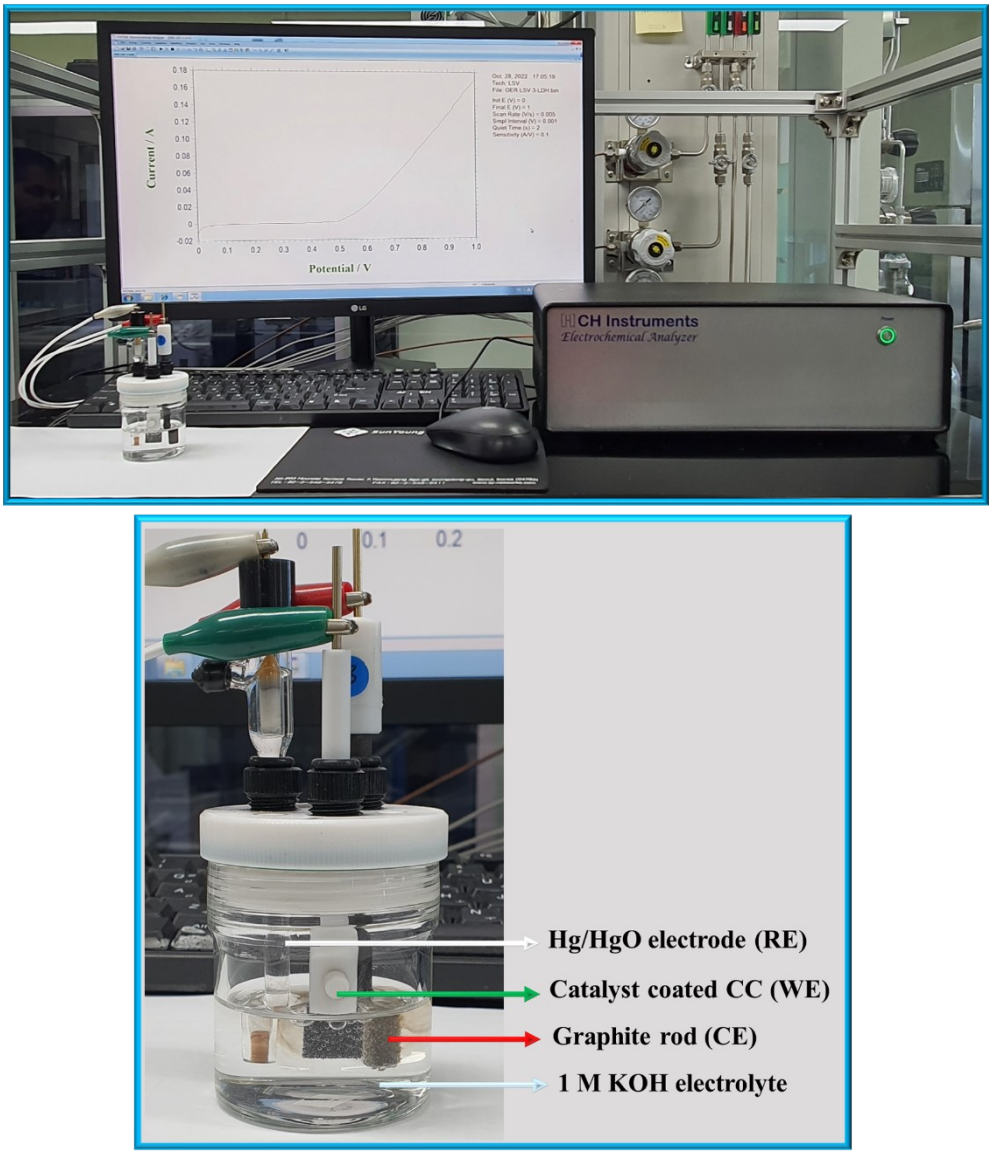

Fig. S10. The photographs of utilized electrochemical setup during the OER measurements of the as-synthesized electrocatalysts with a typical three-electrode configuration in a 1 M KOH electrolyte.

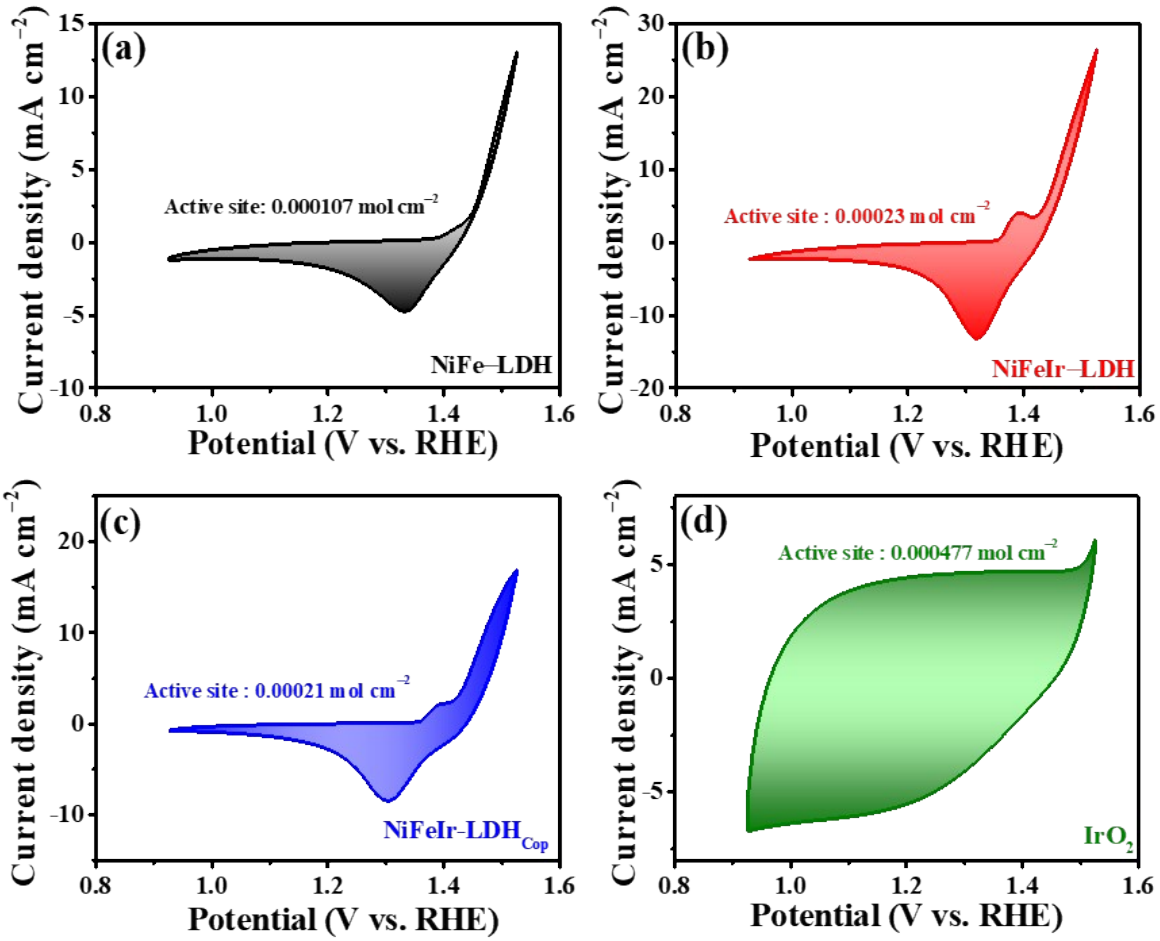

Fig. S11. CV curves of the (a) NiFe-LDH, NiFeIr-LDH, NiFeIr-LDH$_{Cop}$ and commercial IrO_2 samples measured in the potential ranging from 0.926 to 1.526 V vs. RHE at 50 mV s^{-1} for calculate their TOF during the OER.

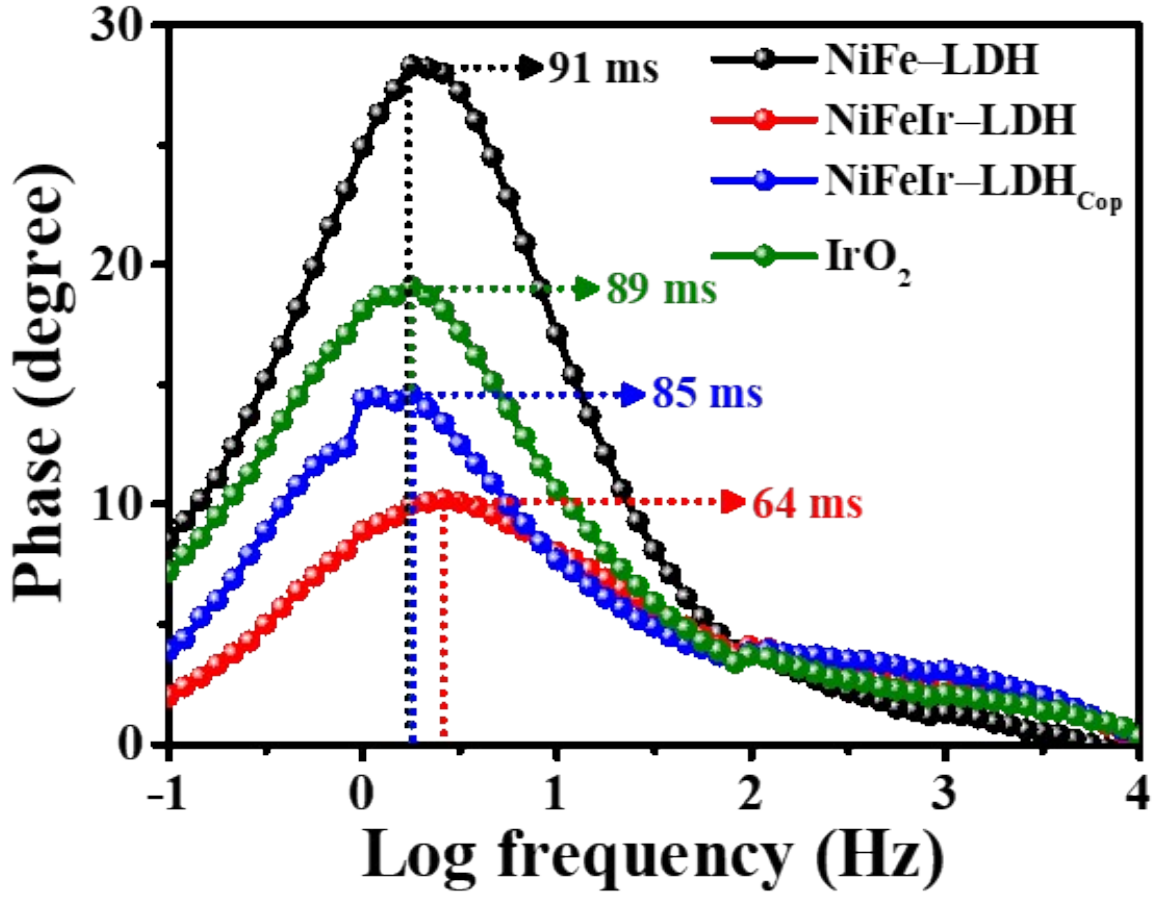

Fig. S12. Bode plots of the (a) NiFe-LDH, NiFeIr-LDH, NiFeIr-LDH_{Cop} and commercial IrO_2 samples measured from the EIS test for the OER.

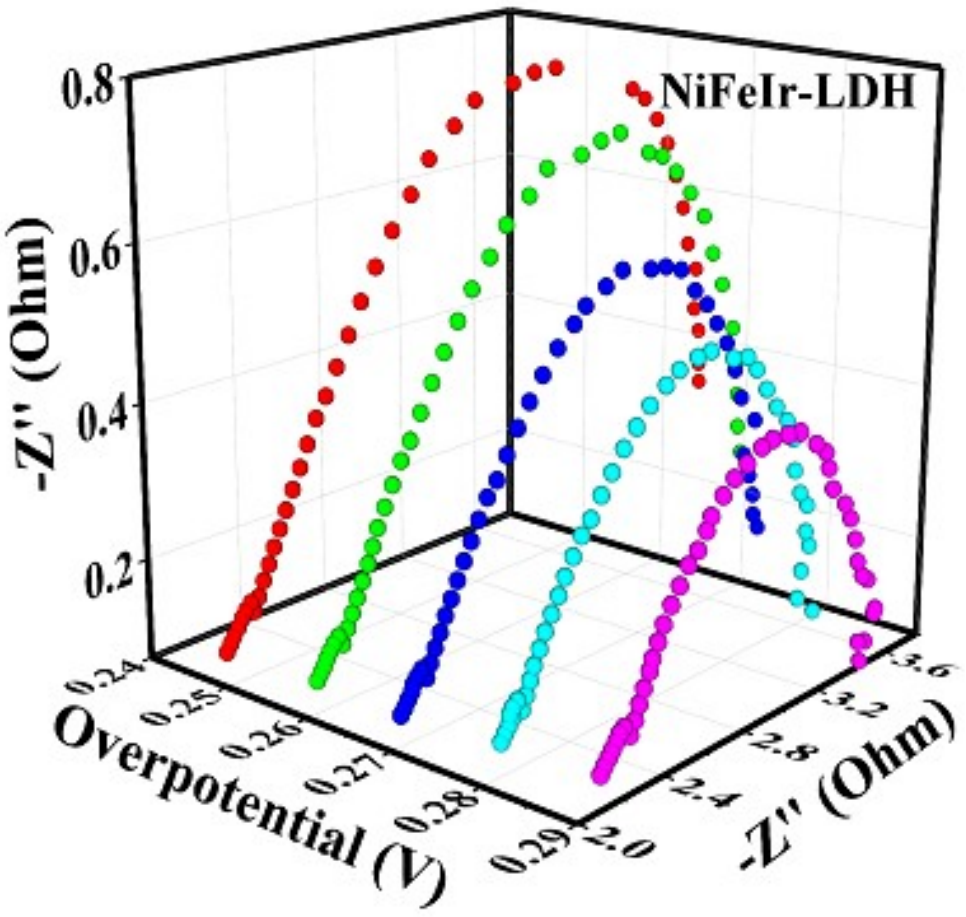

Fig. S13. Nyquist plots of the NiFeIr-LDH nanosheets at various overpotentials from 240 to 290 mV during the OER.

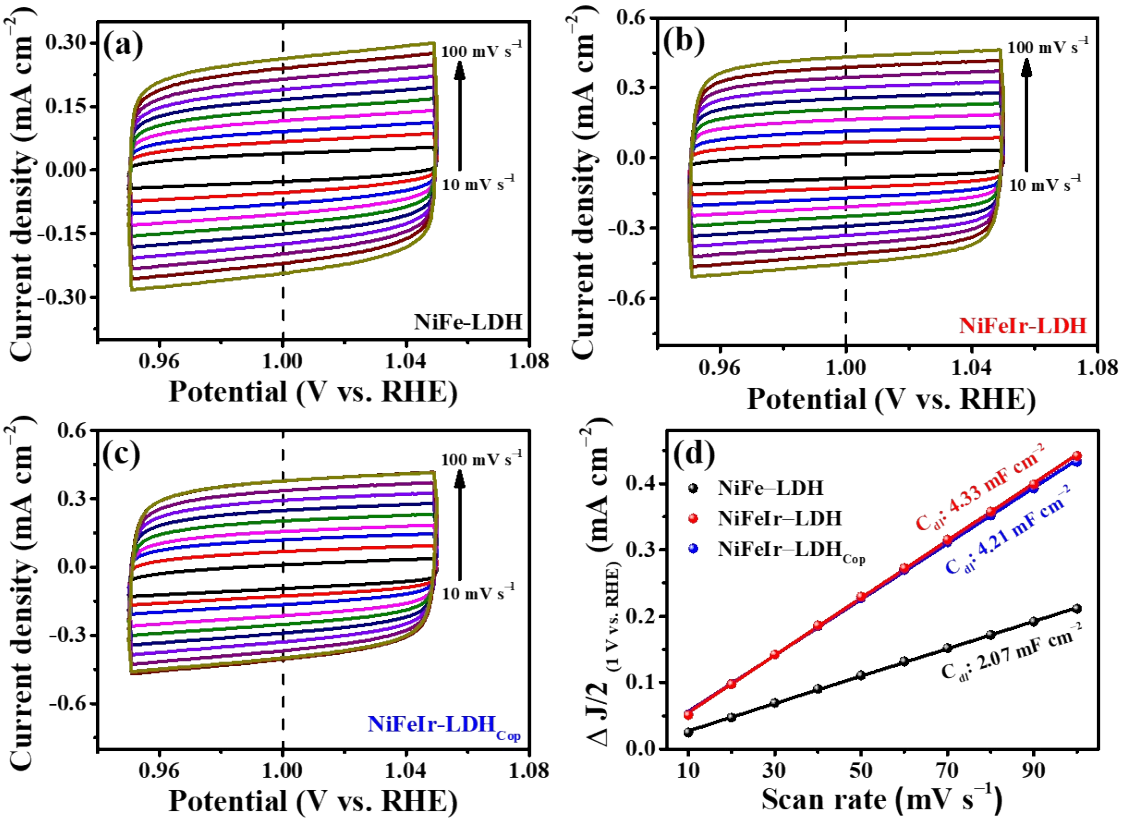

Fig. S14. CV curves of the (a) NiFe-LDH, (b) NiFeIr-LDH and NiFeIr-LDH$_{Cop}$ samples measured in the non-faradic region (0.95 to 1.05 V vs. RHE) at the different scan rates from 10-100 mV s^{-1} for in order to calculate their C_{dl} values. (d) The plots of $\Delta j/2$ at 1.0 V vs. RHE versus the scan rates for the (a) NiFe-LDH, (b) NiFeIr-LDH and NiFeIr-LDH$_{Cop}$ samples with their Cdl vales.

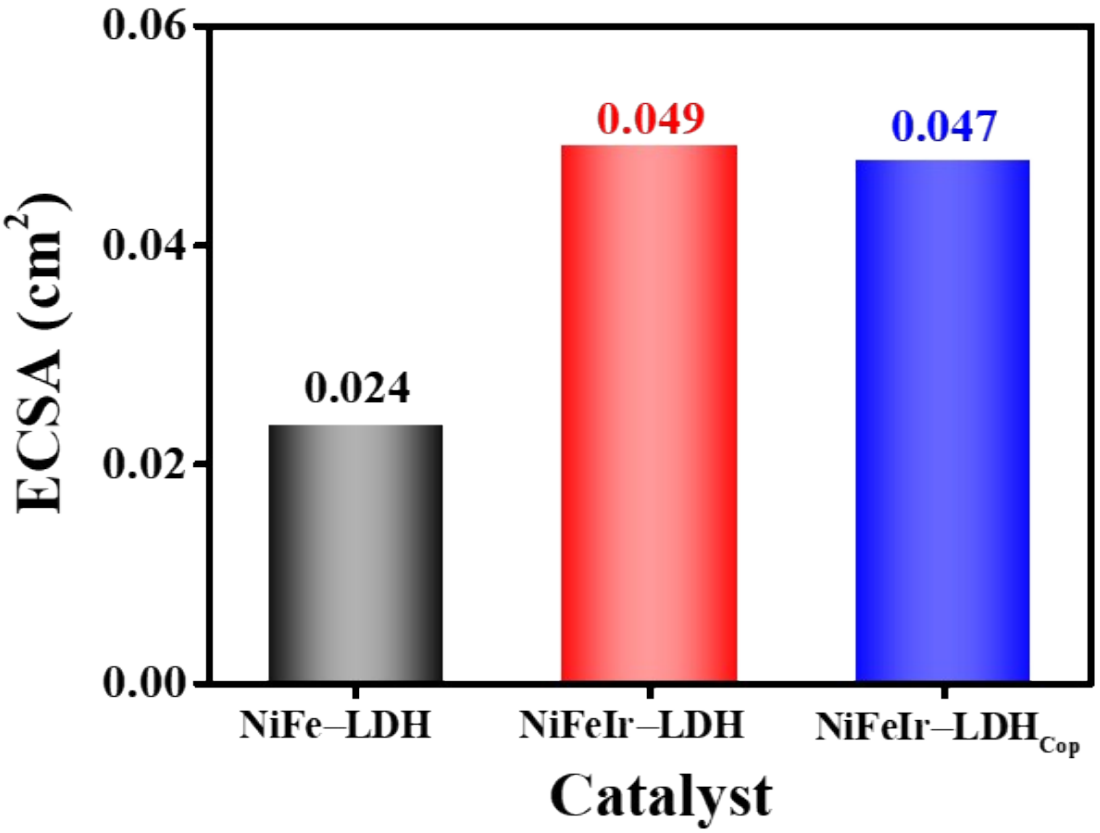

Fig. S15. The calculated ECSA values of the as-synthesized NiFe-LDH, NiFeIr-LDH and NiFeIr-LDH$_{Cop}$ samples.

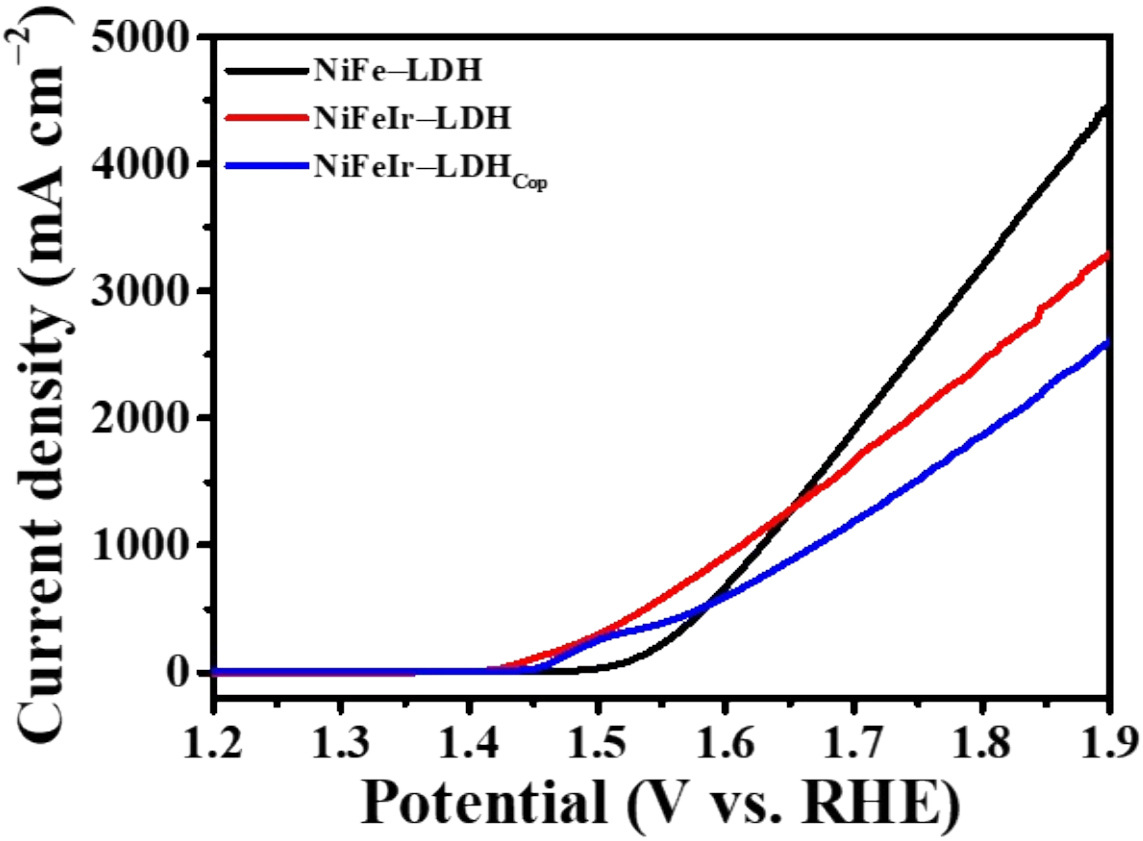

Fig. S16. ECSA normalized LSV curves of the synthesized of the as-synthesized NiFe-LDH, NiFeIr-LDH and NiFeIr-LDH$_{Cop}$ samples.

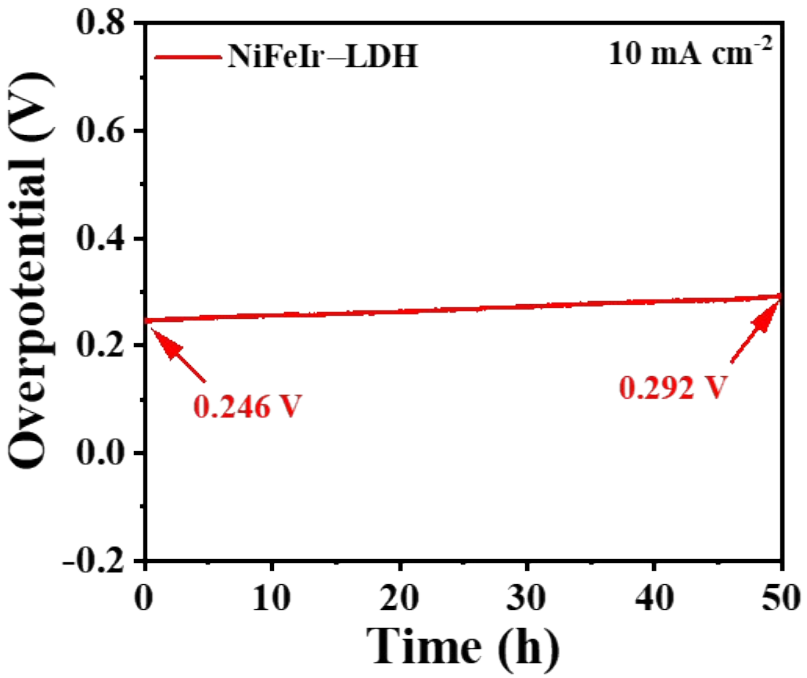

Fig. S17 Long-term OER stability test of NiFeIr-LDH nanosheets at 10 mA cm^{-2} for 50 h.

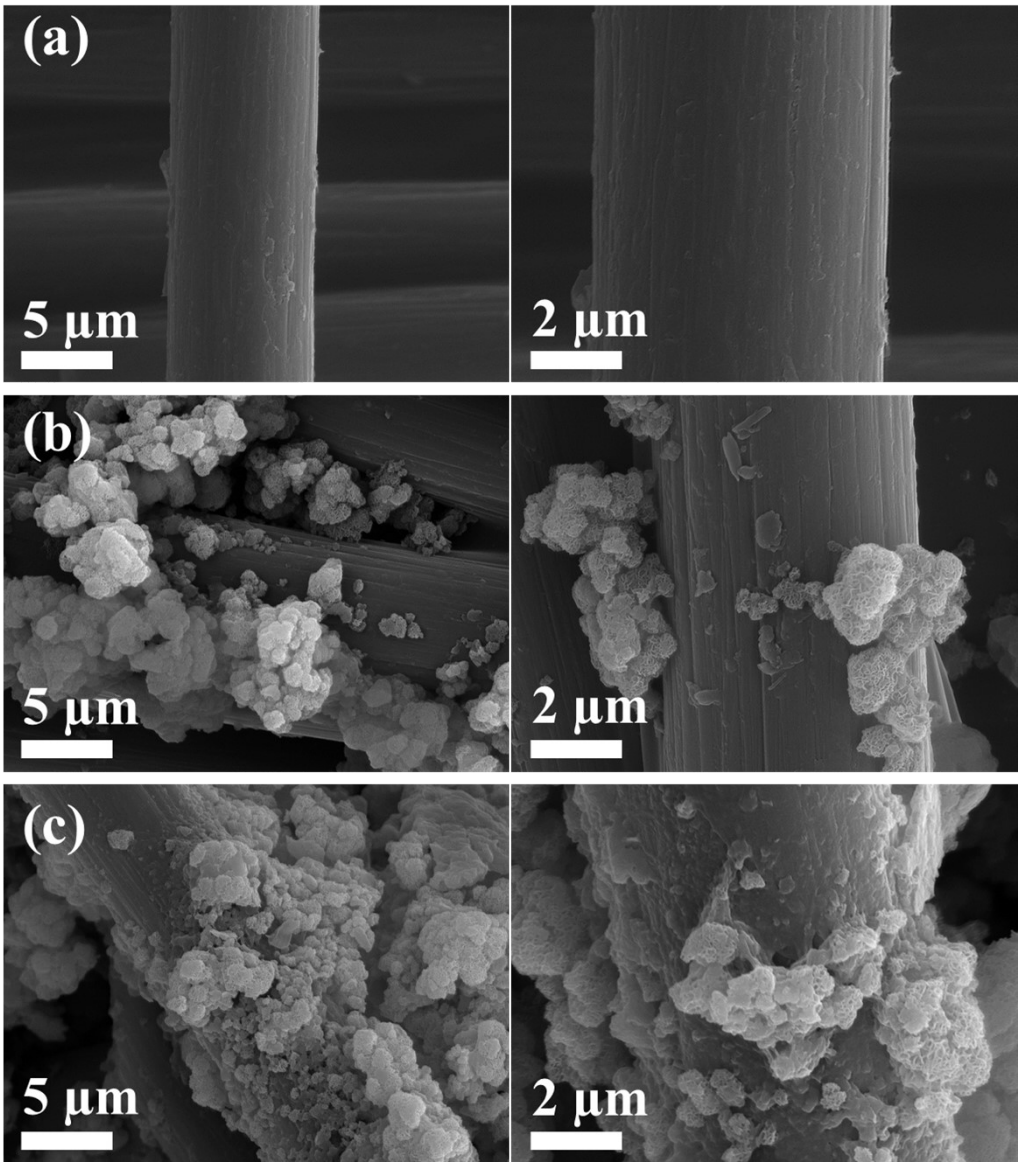

Fig. S18. SEM images of (a) pure CC, (b) NiFe-LDH/CC electrode before OER stability and (c) NiFe-LDH/CC electrode after OER stability for 12 h.

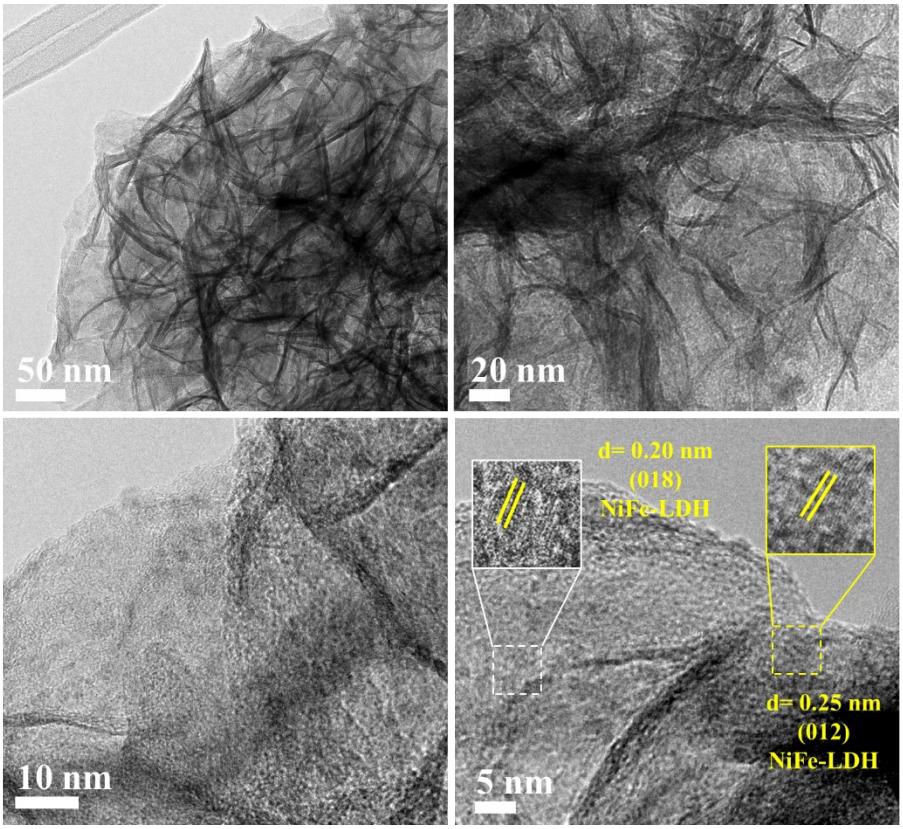

Fig. S19. HR-TEM images of NiFe-LDH after continuous OER stability test for 12 h.

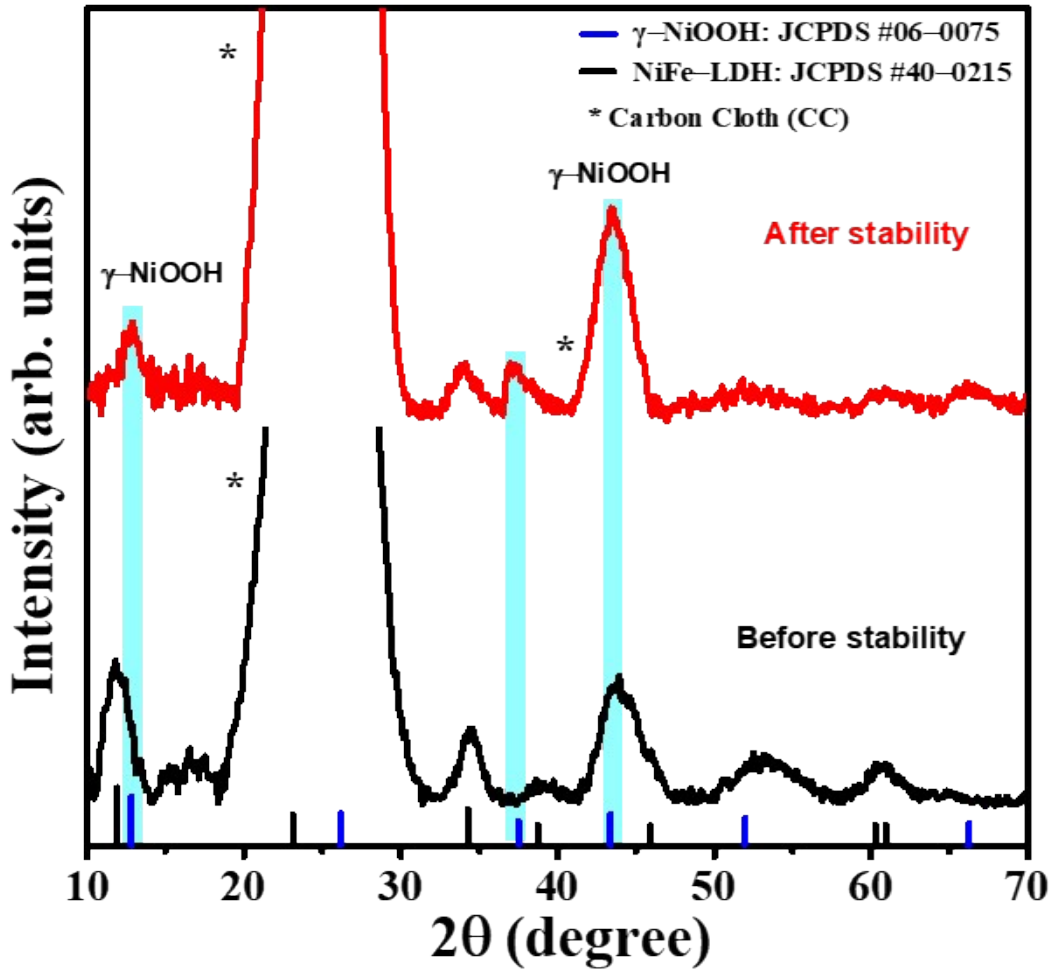

Fig. S20. XRD spectra of NiFe-LDH/CC electrode before and after continuous OER stability test for 12 h.

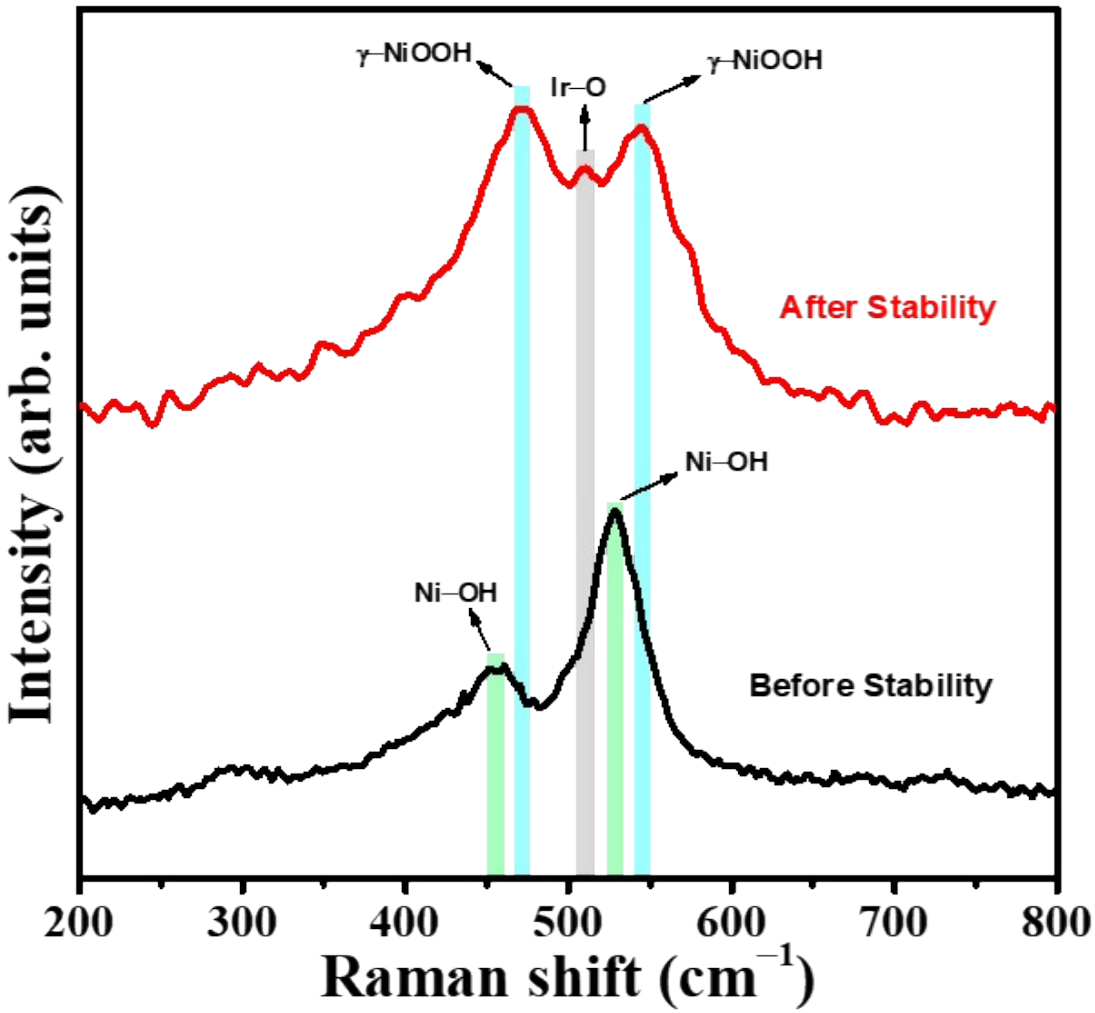

Fig. S21. *Ex-situ* Raman spectra of the NiFe-LDH/CC electrode before and after continuous OER stability test for 12 h.

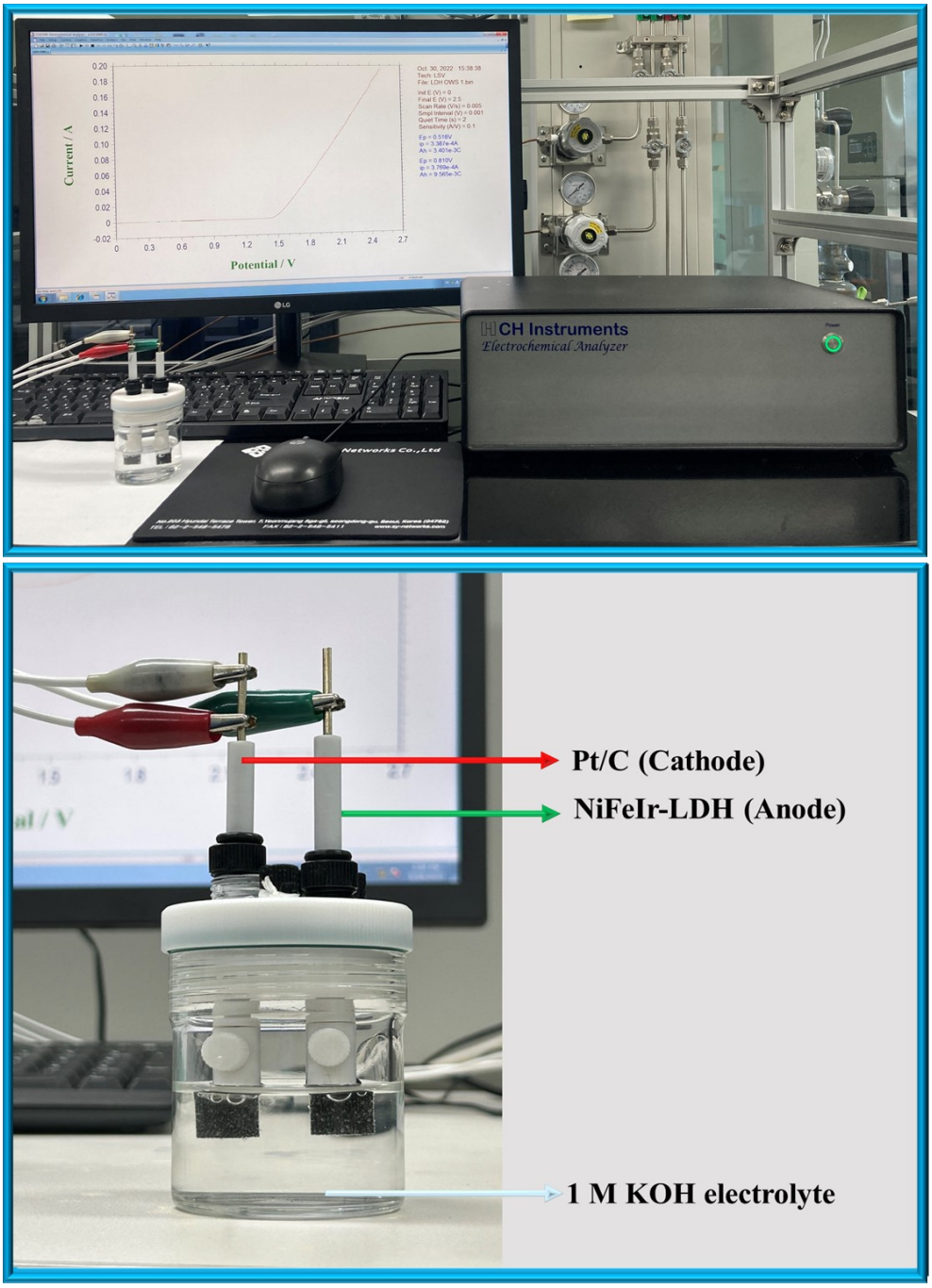

Fig. S22. The photographs of utilized electrochemical setup during the OWS measurements of the as-fabricated NiFeIr-LDH(+)‖Pt/C(-) electrolyzer in a 1 M KOH electrolyte.

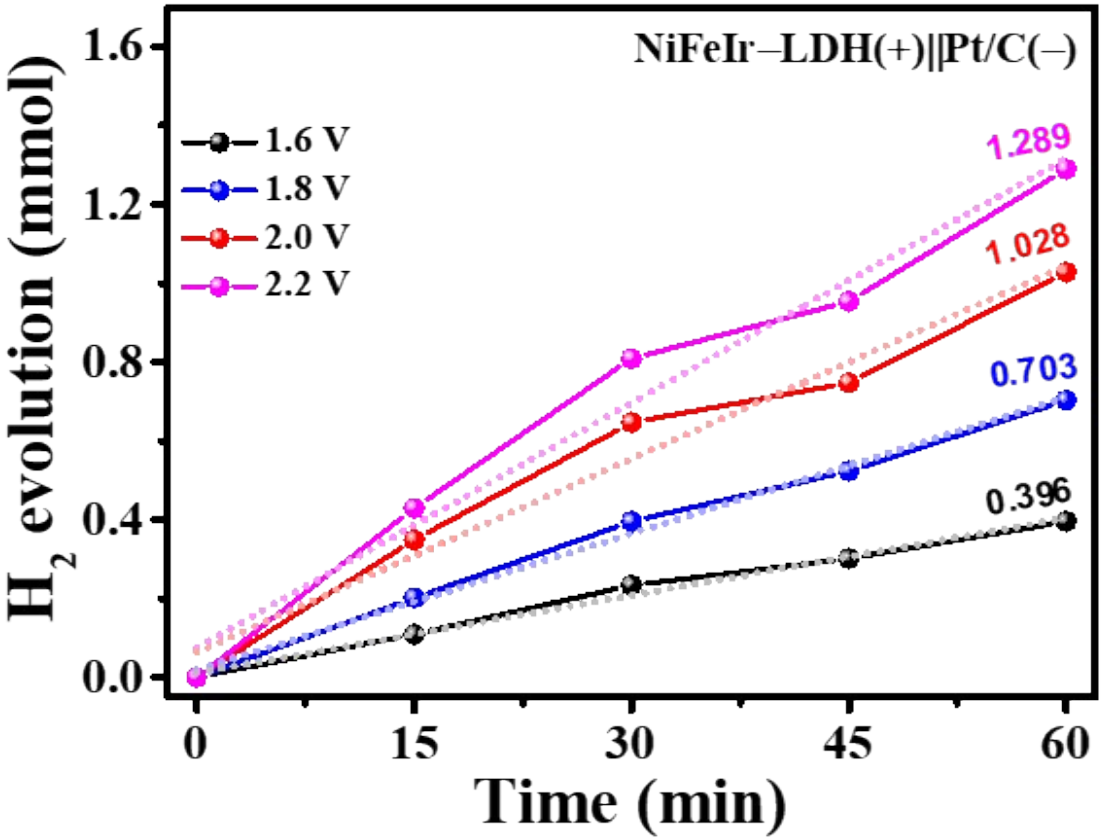

Fig. S23. The amounts of hydrogen production from the NiFeIr-LDH(+) ‖ Pt/C(-) system at applied cell voltages of 1.6, 1.8, 2.0 and 2.2 V.

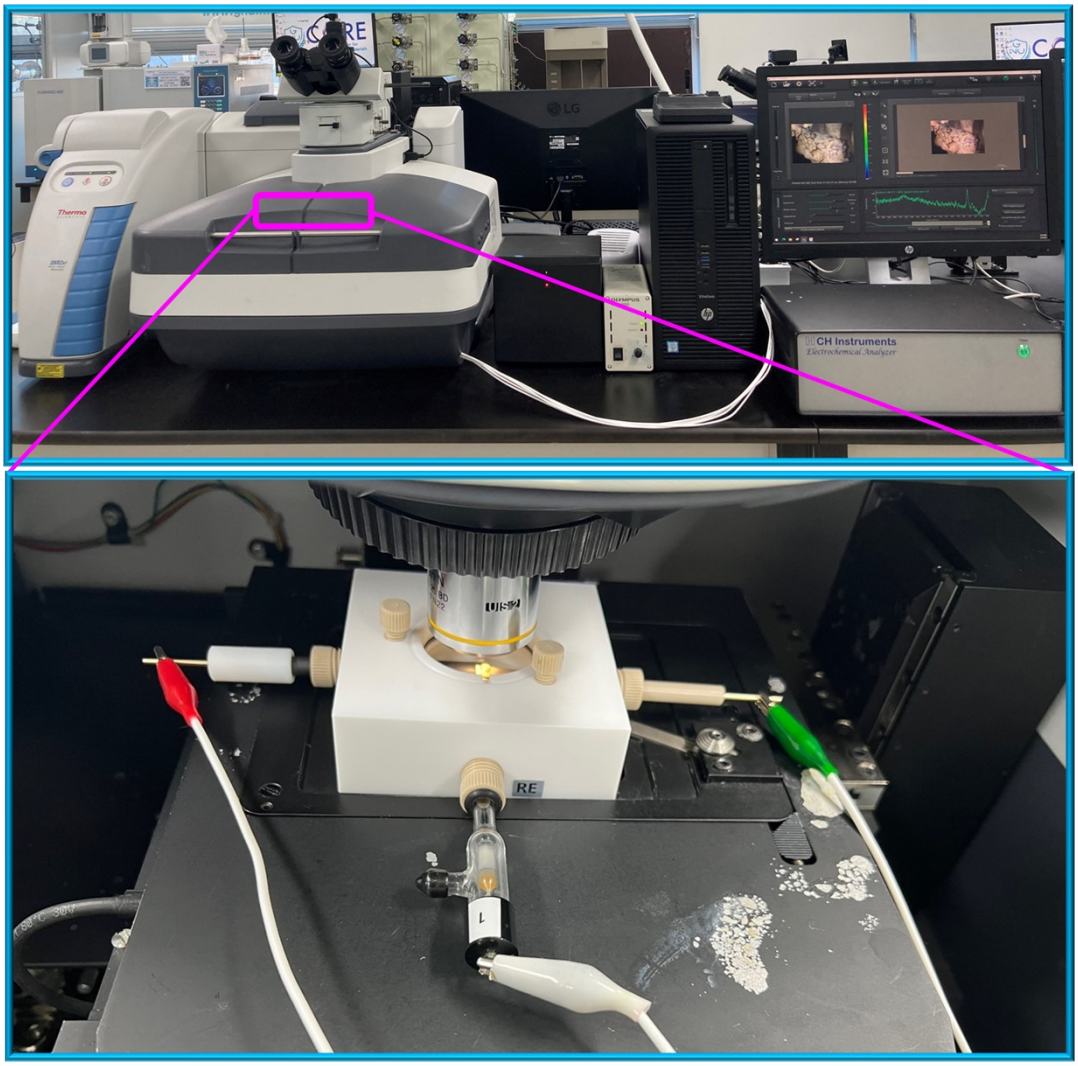

Fig. S24. The photographs of utilized in-situ/operando Raman spectroscopy setup for collecting Raman spectra during the OER.

Table S1. Electrochemical results of the as-synthesized NiFe-LDH, NiFeIr-LDH and NiFeIr-LDH_{Cop} samples.

Electrocatalyst	**OER overpotential (10 mA cm^{-2})**	**OER Tafel slope**	**Charge transfer resistance (R_{ct})**	**Double layer capacitance (C_{dl})**
NiFe-LDH	345 mV	80 mV dec^{-1}	5.83 Ω	2.07 mF cm^{-2}
NiFeIr-LDH	246 mV	46 mV dec^{-1}	1.77 Ω	4.33 mF cm^{-2}
NiFeIr-LDH_{Cop}	261 mV	58 mV dec^{-1}	2.57 Ω	4.21 mF cm^{-2}

Table S2. The comparison of the electrochemical OER performances of as-synthesized NiFeIr-LDH nanosheets from PLI method with those of previously reported OER electrocatalysts in a 1 M KOH electrolyte.

Electrocatalysts	Overpotential (mV)	Current density (mA cm^{-2})	Tafel slope (mV dec^{-1})	Ref.
NiFeIr-LDH	246	10	46	This work
Au/Ir nanochains	300	10	52	[1]
Ir-Co_3O_4@NC	296	10	89	[2]
CuO/RuO_2/C	346	10	85	[3]
Ru@CoFe/D-MOFs	265	10	61	[4]
CoCrRu LDHs	290	10	56	[5]
NiCoFe-LDH	277	10	68	[6]
Mo-NiFe-LDH	471	20	44	[7]
$NiFe_2O_4$/Ti_3C_2	266	10	73	[8]
Ru-CoO	340	10	84	[9]
Ir-doped $NiCo_2O_4$	303	10	78	[10]
ex-Ir-$Ni(OH)_2$	270	10	45	[11]
Ir-ZIF-67@CoFe PBA	269	10	80	[12]
Ir/Ni PNTs	270	10	44	[13]
MXene/NiCo-LDH	340	10	190	[14]
CoFeCr-LDH	278	10	48	[15]
NiCoMn-LDH	248	10	72	[16]
NiFe-LDH@Co/Ni-CNT	267	10	36	[17]
CoFe-LDH	314	10	79	[18]
NiFe-LDH	270	10	48	[19]
$RuCoO_x$@NC	255	10	63	[20]
NiFeCo-LDH	265	10	47	[21]
Ru doped NiCoP	280	10	42	[22]
Fe-doped Co_3O_4/Ru	283	10	79	[23]

Ru@NiCo-MOF HPNs	284	10	78	[24]
Ag NWs@NiFe-LDH	330	10	89	[25]
NiCoFe-LDH	340	10	93	[26]
CoCr LDH/O-CNT	290	10	42	[27]
CoMn-LDH/MWCNT	300	10	73	[28]
ZnCo-LDH/RGO	330	10	73	[29]
CoFe-LDH/g-CN_x	280	10	29	[30]
NiFe-LDH@SWNT	250	10	35	[31]
CoNi-LDH@PCPs	350	10	58	[32]
NiCo-LDH	314	10	77	[33]

References

1. Z. Ke, L. Li, Q. Jia, Y. Yang and H. Cui, *Applied Surface Science*, 2019, **463**, 58-65.
2. S. Jung, R. A. Senthil, C. J. Moon, N. Tarasenka, A. Min, S. J. Lee, N. Tarasenko and M. Y. Choi, *Chemical Engineering Journal*, 2023, **468**, 143717.
3. S. S. Naik, J. Theerthagiri, A. Min, C. J. Moon, S. J. Lee and M. Y. Choi, *Applied Catalysis B: Environmental*, 2023, **339**, 123164.
4. D. Liu, C. Wang, Z. Zhou, C. Ye, R. Yu, C. Wang and Y. Du, *Inorganic Chemistry Frontiers*, 2022, **9**, 6158-6166.
5. C. Dong, X. Zhang, J. Xu, R. Si, J. Sheng, J. Luo, S. Zhang, W. Dong, G. Li, W. Wang and F. Huang, *Small*, 2020, **16**, 1905328.
6. K. Karuppasamy, R. Bose, D. B. Velusamy, D. Vikraman, P. Santhoshkumar, P. Sivakumar, A. Alfantazi and H.-S. Kim, *ACS Sustainable Chemistry & Engineering*, 2022, **10**, 14693-14704.
7. Z. Yin, X. Liu, M. Cui, Z. Cao, A. Liu, L. Gao, T. Ma, S. Chen and Y. Li, *Materials Today Sustainability*, 2022, **17**, 100101.
8. P. V. Shinde, P. Mane, B. Chakraborty and C. Sekhar Rout, *Journal of Colloid and Interface Science*, 2021, **602**, 232-241.

9. H.-W. Wu, Y. Cui, G.-H. Gao, Y.-J. Wang and J.-S. Li, *Journal of Alloys and Compounds*, 2023, **960**, 170847.

10. H.-J. Lee, D.-H. Park, W.-J. Lee, S.-B. Han, M.-H. Kim, J.-H. Byeon and K.-W. Park, *Applied Catalysis A: General*, 2021, **626**, 118377.

11. J. Liu, J. Xiao, Z. Wang, H. Yuan, Z. Lu, B. Luo, E. Tian and G. I. N. Waterhouse, *ACS Catalysis*, 2021, **11**, 5386-5395.

12. W. Liang, C. Wang, J. Li, J. Yin, Z. Wu, S. Li and Y. Du, *Inorganic Chemistry*, 2023, **62**, 20072-20079.

13. Y. Nam, D. Kim, J. Chu, N.-Y. Park, T. G. Kim, K. J. Kim, S.-H. Kim and B. Shin, *Advanced Science*, 2022, **9**, 2104938.

14. Navjyoti, A. K. Sharma, V. Sharma, A. K. Debnath, V. Saxena and A. Mahajan, *Journal of Alloys and Compounds*, 2023, **939**, 168779.

15. L. Qiao, T. Li, Q. Wei, Z. Fu, Z. Cheng, J. Wu, J. Lin, J. Chen, Z. Chen and Y. Qi, *Journal of Physics and Chemistry of Solids*, 2022, **171**, 111015.

16. T. Zhang, H. Huang, J. Han, F. Yan and C. Sun, *ChemElectroChem*, 2020, **7**, 3852-3858.

17. K. Ji, X. Xia, Y. Yue and P. Yang, *Journal of Electroanalytical Chemistry*, 2022, **920**, 116573.

18. Y. Zhang, C. Gan, Q. Jiang, P. Lang, W. Wang and J. Tang, *Materials Science and Engineering: B*, 2022, **282**, 115800.

19. M. Suliman, A. Al Ghamdi, T. Baroud, Q. Drmosh, M. Rafatullah, Z. Yamani and M. Qamar, *International Journal of Hydrogen Energy*, 2022, **47**, 23498-23507.

20. R. A. Senthil, S. Jung, A. Min, C. J. Moon and M. Y. Choi, *Chemical Engineering Journal*, 2023, **475**, 146441.

21. A. C. Thenuwara, N. H. Attanayake, J. Yu, J. P. Perdew, E. J. Elzinga, Q. Yan and D. R.

Strongin, *The Journal of Physical Chemistry B*, 2018, **122**, 847-854.

22. J. Kim, B. J. Min, T. Kwon, T. Kim, H. C. Song, H. C. Ham, H. Baik, K. Lee and J. Y. Kim, *Chemistry – An Asian Journal*, 2021, **16**, 3630-3635.

23. L. Gao, X. Zhong, J. Chen, Y. Zhang, J. Liu and B. Zhang, *Chinese Chemical Letters*, 2023, **34**, 108085.

24. D. Liu, H. Xu, C. Wang, H. Shang, R. Yu, Y. Wang, J. Li, X. Li and Y. Du, *Inorganic Chemistry*, 2021, **60**, 5882-5889.

25. X. Zhang, A. N. Marianov, Y. Jiang, C. Cazorla and D. Chu, *ACS Applied Nano Materials*, 2020, **3**, 887-895.

26. L. Qian, Z. Lu, T. Xu, X. Wu, Y. Tian, Y. Li, Z. Huo, X. Sun and X. Duan, *Advanced Energy Materials*, 2015, **5**, 1500245.

27. B. Malik, H. K. Sadhanala, S. K. T. Aziz, S. Majumder, R. Konar, A. Gedanken and G. D. Nessim, *ACS Applied Nano Materials*, 2022, **5**, 4091-4101.

28. G. Jia, Y. Hu, Q. Qian, Y. Yao, S. Zhang, Z. Li and Z. Zou, *ACS Applied Materials & Interfaces*, 2016, **8**, 14527-14534.

29. D. Tang, Y. Han, W. Ji, S. Qiao, X. Zhou, R. Liu, X. Han, H. Huang, Y. Liu and Z. Kang, *Dalton Transactions*, 2014, **43**, 15119-15125.

30. T. Bhowmik, M. K. Kundu and S. Barman, *ACS Applied Energy Materials*, 2018, **1**, 1200-1209.

31. H. Liu, J. Zhou, C. Wu, C. Wang, Y. Zhang, D. Liu, Y. Lin, H. Jiang and L. Song, *ACS Sustainable Chemistry & Engineering*, 2018, **6**, 2911-2915.

32. W. Wang, Y. Lu, M. Zhao, R. Luo, Y. Yang, T. Peng, H. Yan, X. Liu and Y. Luo, *ACS Nano*, 2019, **13**, 12206-12218.

33. S. Sun, C. Lv, W. Hong, X. Zhou, F. Wu and G. Chen, *ACS Applied Energy Materials*,

2019, **2**, 312-319.